Applied Catalysis B: Environmental 160–161 (2014) 574–581

Contents lists available at ScienceDirect

Applied Catalysis B: Environmental

journal homepage: www.elsevier.com/locate/apcatb

Study of the effect of addition of In to Pt-Sn/γ-Al_2O_3 catalysts for high purity hydrogen production via partial dehydrogenation of kerosene jet A-1

Elia Gianotti, Álvaro Reyes-Carmona, Mélanie Taillades-Jacquin*, Gilles Taillades, Jacques Rozière, Deborah J. Jones

Institut Charles Gerhardt UMR 5253, Agrégats, Interfaces et Matériaux pour l'Energie, Université Montpellier 2, Place Eugène Bataillon, 34095 Montpellier Cedex 5, France

ARTICLE INFO

Article history:
Received 7 April 2014
Received in revised form 5 June 2014
Accepted 6 June 2014
Available online 13 June 2014

Keywords:
Hydrogen production
Indium-Pt-Sn/γ-Al_2O_3
Partial dehydrogenation
Kerosene jet A-1
Carbon coke

ABSTRACT

The partial dehydrogenation (PDh) of hydrocarbons is emerging as a promising technology for high purity H_2 production, suitable to directly feed a fuel cell stack. In particular for direct on-board application this method has the advantage of avoiding the problem of gaseous or liquid hydrogen storage and allows the recovery of the dehydrogenated hydrocarbons for valuable usage. Partial dehydrogenation of hydrocarbon blends like kerosene could be a convenient way to increase the energy efficiency in aviation on-board applications. A series of trimetallic catalysts (1%Pt-1%Sn-[*x*]%In/γ-Al_2O_3 with $x = 0.25, 0.5, 0.75, 1$) has been prepared for low sulfur kerosene dehydrogenation. Particularly remarkable is the enhancement of activity and stability observed for In/Pt/Sn weight ratio of 0.5:1:1 which provides an average H_2 production of 2900 NL h^{-1} kg_{cat}^{-1} (86.7 NL $L_{kerosene}^{-1}$), sufficient to produce ≈2.9 kW of electricity. The hydrogen yield achieved is 6.4% w/w with a TOF (turnover factor) of 0.69 s^{-1}.

1. Introduction

Increasing the efficiency in transportation technologies is essential for a sustainable development. The search for alternative power sources with low pollutant emissions and affordable cost is driving a great research effort in the last decade [1,2]. In this context, fuel cells are a very attractive technology due to their high efficiency, making them a strong candidate for the integration into the energy system. A key problem for their employment, especially for transportation and on-board applications, is the storage of the hydrogen fuel [3]. Currently physical storage devices like cryogenic liquid H_2 tanks or highly compressed gaseous H_2 tanks are the closest to the DOE (U.S. Department of Energy) and European specifications but they have some drawbacks: compressed H_2 needs a large volume tank (depending on the pressure in the tank) and the higher the tank pressure, the thicker has to be the tank. Liquid H_2 has a lot of evaporation losses and needs a high amount of energy for the liquefaction [4,5]. Other technologies such as chemical storage using hydrogen absorbing alloys or organic hydrides are gaining increasing interest as they can avoid the problems associated with liquid and high pressure storage. Chemical storage via hydrogenation/dehydrogenation of liquid hydrocarbons is increasingly considered a viable method and, in addition, the absence of oxygen in the process of hydrocarbons dehydrogenation makes it suitable for producing a hydrogen stream free of CO, which can be used directly to feed a fuel cell stack, potentially without further purification or treatment [6–8].

Partial dehydrogenation of hydrocarbon blends like kerosene could be a convenient way to achieve lower emissions in aviation applications and contribute to higher energy efficiency. On-board electricity generation is supplied by the auxiliary power unit (APU) (90 kW based on Airbus A320 data) and is currently generated with a turbine [9]. The implementation of a dehydrogenation reactor coupled with a fuel cell system for electricity generation instead of the turbine would lead to many advantages: typical turbine efficiency for kerosene to electricity conversion is only 15% and can be enhanced; partially dehydrogenated kerosene can be recycled to the engines; fuel cell emissions are not contaminant which would reduce air traffic pollution [10].

A significant number of supported-metal catalysts have been developed for hydrocarbon dehydrogenation, and the most widely used are based on supported Ni or Pt often in combination with other metals. The properties of the support also have a great importance: acidity, pore size and pore volume are crucial factors that

* Corresponding author. Tel.: +33 467144620; fax: +33 467143304.
E-mail address: melanie.taillades-jacquin@univ-montp2.fr (M. Taillades-Jacquin).

http://dx.doi.org/10.1016/j.apcatb.2014.06.003
0926-3373/

strongly affect the catalyst performance [8,11–20]. For gas-phase kerosene partial dehydrogenation in particular, there are already a few examples of the use of the catalytic system based on Pt-Sn/Al_2O_3 showing encouraging results with kerosene surrogates. Nevertheless, the deactivation rate of the catalyst is still very high when the reagent used is a real commercial kerosene jet A-1 with lifetimes in the range of few hours [21–25]. Lucarelli et. al. [23] show how the majority of the hydrogen produced comes from the conversion of cyclo-alkanes leaving the linear paraffins, which are the primary component of kerosene (around 65% vol.), almost unconverted. Those preliminary studies indicate that the overall conversion of hydrocarbons is sufficiently low to allow the reutilisation of the dehydrogenated product as fuel. As reported in previous studies, the optimal Pt-Sn ratio for this reaction giving a good compromise between hydrogen productivity and catalyst stability is around 1:1 w/w. The acidity of the catalyst is an important factor, as high content of strong acid sites shifts the selectivity towards undesired cracking reaction and formation of coke [26,27]. The importance of kerosene sulfur content is also a key parameter to consider, as this element is a poison for many catalyst active phases [26]; for this reason in the present study a low sulfur content commercial jetA-1 kerosene (ULSK) has been used in order to focus on the deactivation by carbon coke deposition.

The catalyst system based on Pt-Sn supported on γ-Al_2O_3 is well-known and widely used in various processes of reforming and dehydrogenation: amongst these, naphtha reforming is one of the more frequent [28,29] together with paraffin to olefin dehydrogenations [27,30,31]. It is demonstrated that the addition of a third metal to Pt-Sn/Al_2O_3 can lead to improvement of the catalytic properties, and examples of enhanced trimetallic catalysts for reforming or dehydrogenation can be easily found (Pt-Sn-M/Al_2O_3 M = Re, Ir, Ge) [32–34]. However, the literature concerning the effect and interaction of In with the Pt-Sn for dehydrogenation reaction is very limited. One of the rare examples, reported by Bocanegra et al. [35] that carried out a study on Pt-Sn-In/$MgAl_2O_3$ catalysts for n-butane dehydrogenation, shows that indium addition remarkably enhances the catalyst stability and inhibits undesired hydrogenolysis reactions.

In this work the effect of addition of In to Pt-Sn/γ-Al_2O_3 catalysts has been investigated by synthesising a series of catalysts with increasing In loading and evaluating the material properties by several characterisation techniques (X-Ray diffraction, X-Ray fluorescence, NH_3 temperature programmed desorption, H_2 temperature programmed reduction, adsorption–desorption of N_2 and H_2 chemisorption) comparing them to a Pt-Sn catalyst as reference. The catalysts have been tested on a laboratory scale plant for the reaction of partial dehydrogenation of low sulfur jetA-1 reaction, analysing the role of In on Pt dehydrogenation activity and on catalyst lifetime. The mechanisms of catalyst deactivation have also been studied by analysis on the carbon coke produced during the reaction using Raman spectroscopy, elemental analysis and thermo-gravimetric analysis.

2. Materials and methods

2.1. Catalyst preparation

A series of catalysts containing equal amounts of Pt-Sn (1%Pt, 1%Sn w/w) and a range of In contents (0.25%, 0.5%, 0.75%, 1% w/w) has been prepared by the incipient wetness impregnation technique, using as support a commercial γ-Al_2O_3 (*Sasol Puralox SCFa40*). Indium was added using aqueous solutions with an $InCl_3$ (*Alfa Aesar*) concentration of 0.0243 M; 0.0486 M; 0.0731 M; 0.0978 M, respectively for the 0.25%, 0.5%, 0.75%, 1% w/w, followed by drying at 80 °C. Subsequently Pt and Sn were added by co-impregnation to the previously obtained In/Al_2O_3 using aqueous solutions of $H_2PtCl_6{\cdot}6H_2O$ (*Alfa Aesar*) and $SnCl_2{\cdot}2H_2O$ (*Acros*), to give a ratio 1% wt. Pt and 1% wt. Sn (mol. ratio Pt/Sn = 0.61). The tin precursor was dissolved in 1 M HCl and then mixed with the platinum salt solution upon which the solution turns red-brown due to the formation of a $[PtCl_2(SnCl_3)_2]^{2-}$ complex. In the literature it is reported that the procedure of Pt-Sn co-impregnation leads to a higher amount of Pt_xSn alloy formation that lead to improved catalyst stability [36,37]. After drying the impregnated materials overnight at 80 °C, they were thermally treated in air at 120 °C for 2 h and then at 560 °C for 2 h (heating ratio 2 °C min^{-1}). The catalysts were labelled as "Cat-In[*x*]" where *x* is the percentage in weight of indium. A reference Pt-Sn bimetallic catalyst without In was also synthesised with the same procedure and it was labelled as "Cat-Ref".

2.2. Characterisation techniques

Structural investigation of the samples was performed by X-Ray diffraction (XRD), using a *PANalyticalX'Pert* diffractometer, with CuK_α as radiation source (λ = 0.15418 nm, 40 kV, 25 mA); the acquisition time was 60 min. Phase identification was performed using *HighScore* software by *PANalytical*.

Chemical composition verification of the samples was performed by X-Ray fluorescence (XRF) using a *PANalytical AXIOS MAX* instrument, with a Rh radiation source (4 kW). Elemental quantification was performed using *SUPER-Q* software.

Adsorption–desorption N_2 isotherms were carried out at −196 °C with an *ASAP2020* system from *Micromeritics*. Samples were out-gassed at 200 °C for 8 h under a vacuum of 66.7 Pa. Specific surface area was calculated using the BET (Brunauer, Emmett and Teller) method and pore size distribution using the BJH (Barrett, Joyner, Halenda) method using the *ASAP2020* implemented software; pore volume values are related to the condensation point at $P/P^0 = 0.99$.

The acidity of the materials was studied by NH_3 temperature programmed desorption (NH_3-TPD), using an *Autochem 2910* automatic system from *Micromeritics*. Samples were heated to 550 °C in a He flow of 30 ml min^{-1} (heating ratio 5 °C min^{-1}) then cooled to 100 °C. Then a flow of 20 ml min^{-1} pure NH_3 was passed through the samples for 1 h, which were then flushed with He at 100 °C for 1 h. NH_3 was thermally desorbed up to 600 °C with a heating ramp of 10 °C min^{-1} and the signal was registered using a TC (thermal-conductivity) detector. The apparatus was calibrated using $Ni(NH_3)_6Cl_2$ as NH_3 source.

H_2 temperature programmed reduction (H_2-TPR) war performed in an *Autochem 2910* apparatus. The samples were oxidised in synthetic air (30 ml min^{-1}; 500 °C, 5 °C min^{-1}), then after cooling to 50 °C, a 30 ml min^{-1} flow of H_2(5%)/N_2 mixture was passed over the sample, which was then heated at 10 °C min^{-1} up to 700 °C, registering the H_2 consumption with a TC detector.

H_2 chemisorption was performed in an *Autochem 2910* apparatus. The samples were heated in air flux (30 ml min^{-1}; 500 °C, 5 °C min^{-1}) and then reduced with a H_2(5%)/N_2 mixture at 350 °C. Desorption of physisorbed hydrogen was carried out in N_2 flow at 380 °C for 1 h. Pure H_2 pulses adsorption was recorded at 40 °C. The stoichiometry assumed for the dispersion calculation was $Pt/H_2 = 2$ and for the particles size calculation the shape considered was a hemisphere.

Thermo-gravimetric analyses on deactivated catalysts were performed using a *Netzsch* STA409TP TG/DTA system, working in dynamic-air flux mode. Before the analysis, samples were out-gassed overnight to eliminate any residue of volatile products in the samples. The thermal programme (1 h standby at 60 °C then up to 800 °C), was performed under a flow of synthetic air of 50 ml min^{-1}, with a ramp of 5 °C min^{-1}.

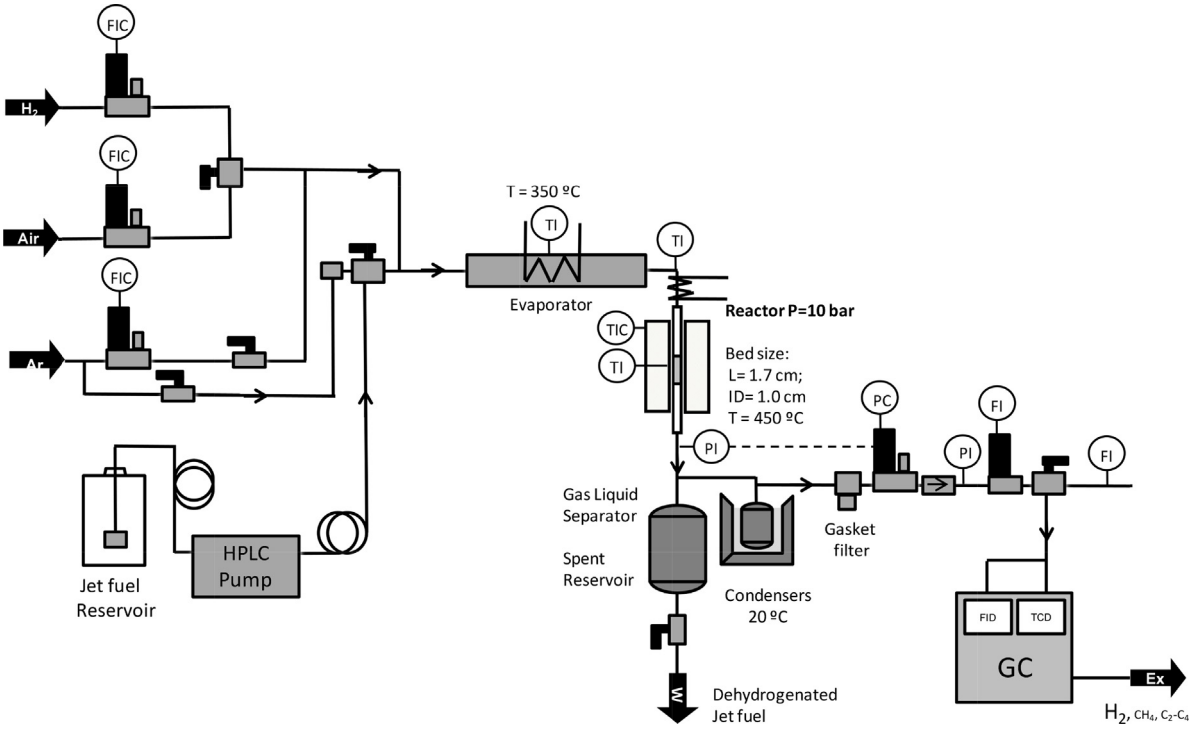

Fig. 1. Laboratory scale bench test scheme.

CNHS Elemental analysis on spent catalysts was performed with a *ThermoFinnigan Flash EA1112* automatic analyser.

The identification of baselines and the deconvolution of data were made with the analytic software *Fityk* (v. 0.9.8) using a Gaussian as model function for the peaks curve and the Levenberg-Marquardt method of fitting calculations.

2.3. Catalytic testing of kerosene PDh reaction

The PDh reaction on low sulfur content kerosene jet A-1 (S < 3 ppm), was performed in a stainless steel fixed-bed tubular reactor. Before the reaction, the catalysts were oxidised in synthetic air flow (55 ml min^{-1}) at 500 °C and reduced in a H_2/Ar flow (55 ml min^{-1}—4:6 v/v) at 350 °C and atmospheric pressure for 2 h. The kerosene was brought with a volumetric pump (*Shimatzu* LC20AD—0.53 ml min^{-1}) to the evaporator and then kerosene vapour (93% vol.) was mixed with a 7% vol. of H_2 (used to simulate a recycle) before entering the reactor containing pelletised catalyst (d = 1–0.85 mm; $V_{cat.bed}$ = 1.8 cm^3; mass average ≈1 g) at T = 450 °C (previous work shows that this is the optimal T for the reaction [23]) and P = 10 bar. These flows were regulated in order to obtain a contact time τ = 2 s (calculated at standard temperature and pressure). A scheme of the reaction rig is shown in Fig. 1. After condensation of the dehydrogenated kerosene, hydrogen production (NL h^{-1} kg_{cat}^{-1}) was calculated from measurement of the gas out-flow with a digital mass flow meter (*Brooks5860S1 Smart II* mass flow meter), and the data processed with *LabView 8.2* instrumentation software. Hydrogen production was calculated following the equation (Eq. (1)):

$$H_2 \text{ production rate} = \frac{\text{Produced Gas OutFlow (NL/h)} - \text{Hydrogen Flow Recycle simulation (NL/h)}}{m_{cat}\,(\text{kg})} \quad (1)$$

Hydrogen purity was analysed with a gas chromatograph *Agilent7890A* equipped with a dual column system. A *HP-PLOTmolesieve 5A column* connected to a Thermal Conductivity Detector (TCD) was used to analyse the composition of the gas-phase produced by the reaction (hydrogen, methane, propane) and *a HP-PLOT/Q column* with a Flame Ionisation Detector (FID) to analyse the traces of light hydrocarbons (C4–C5) present in the gas stream. Hydrogen yield is calculated as ratio between hydrogen produced and total amount of hydrogen in the kerosene used for the reaction (w/w). Catalyst lifetime is calculated by linear extrapolation of the H_2 productivity curves between 180 and 360 min of TOS (time on stream). Deactivation % is calculated from the ratio between initial and final H_2 productivity.

3. Results and discussion

3.1. Structural and surface characterisation

In Fig. 2 some of the most significant XRD patterns are reported. All the materials show the typical diffractions lines of γ-Al_2O_3 but there is no appreciable difference between the diffraction pattern of the Al_2O_3 support and those of fresh catalysts. In fact, none of the catalysts exhibit peaks attributable to Pt crystalline phases; this could be due to factors such as the low platinum content and high dispersion of the metals. From observation of the XRD patterns the only noticeable difference is between fresh and spent material, the latter present peaks characteristic of graphite carbon (25 and 42°2θ).

In Table 1 the composition of the catalysts measured by XRF analysis is summarised, showing a comparable amount of Pt and Sn for all materials. The nominal value is 1% w/w for both Pt and Sn and the results are close to this for Pt (average 1.0% w/w) and slightly lower for Sn (average 0.6% w/w). The In contents measured are also lower than the nominal amount impregnated, possibility due to the method used for the integration: the values are calculated using calibrations for the reduced metal (oxidation state zero) while (particularly for Sn), the average oxidation state may

Table 1
Fresh materials characterisation parameters.

Material	Pt (%)[a]	Sn (%)[a]	In (%)[a]	Metallic dispersion (%)[b]	Metal particles size (nm)[b]	Total acidity (μmol NH_3/g)[c]
Al_2O_3	–	–	–	–	–	127.1
Cat-Ref	0.92	0.63	0.00	48.7	2.3	126.0
Cat-In[0.25]	0.97	0.61	0.13	43.4	2.6	132.0
Cat-In[0.5]	1.05	0.65	0.24	49.3	2.3	123.5
Cat-In[0.75]	0.96	0.63	0.34	41.3	2.7	120.0
Cat-In[1]	1.00	0.57	0.49	35.7	3.2	117.7

[a] XRF.
[b] H_2-chemisorption.
[c] NH_3-TPD.

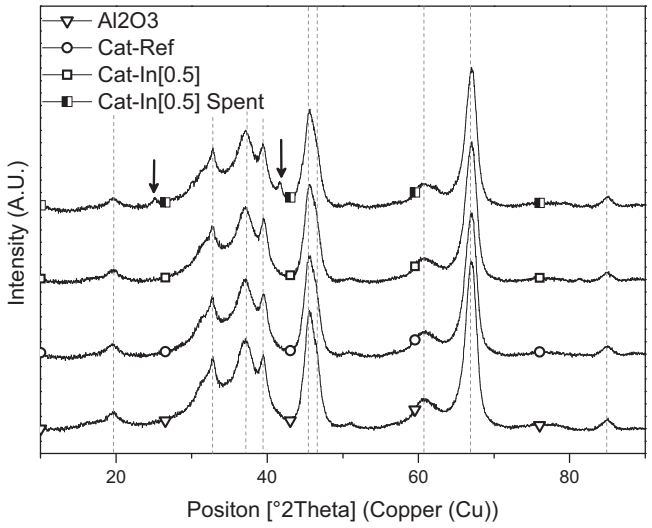

Fig. 2. XRD patterns of the alumina support and some of the catalysts (- - - grey dotted lines: γ-Al_2O_3; ↓ down arrow: carbon coke).

be higher. Overall the values indicate a good reproducibility of the impregnation method.

Porosity data for the materials are reported in Table 2. The calcined original mesoporous γ-Al_2O_3 used as support has a surface area of 173 $m^2\,g^{-1}$ with a narrow pore diameter distribution centred at 10 nm. All the catalysts display similar values of surface area, slightly lower than the surface area of the non-impregnated Al_2O_3 support (Fig. 3A). The values for the catalysts are in the range of 157–168 $m^2\,g^{-1}$ of surface area and pore diameter centred at 9.6–10.2 nm. As expected the addition of metals leads to a slight diminution of the porosity, but it is noticed that the pore diameter distribution remains monomodal and very narrow (Fig. 3B). The surface and porosity analysis performed on the spent materials after reaction (Fig. 3C) all exhibit a similar decrease of the total surface area (≈8%), due to carbon coke deposition (Table 1). No changes in pore diameter are seen between fresh and spent materials (Fig. 3D) meaning that the majority of the pores are still accessible and have not been clogged by the carbon coke formed.

Table 2
Surface area and porosity analysis.

Material	BET surface area (m^2/g)	BJH_{des} pore diameter (nm)	BJH_{des} pore volume (cm^3/g)	Spent material surface area (m^2/g)
Al_2O_3	173	10.0	0.61	–
Cat-Ref	168	10.2	0.57	151
Cat-In[0.25]	165	10.0	0.53	153
Cat-In[0.5]	162	9.8	0.53	149
Cat-In[0.75]	157	9.6	0.52	147
Cat-In[1]	162	9.7	0.52	152

The analysis of surface acidity was performed on the catalysts and on the calcined support via desorption of NH_3 and the results are shown in Fig. 4. The curves have been integrated dividing the desorption in three zones: the first one attributed to weak acid sites (0–250 °C), the second attributed to medium acidic sites (250–350 °C) and the third one to the strong acid sites (350–600 °C). Those values of ammonia desorption temperatures are similar to previous reports in the literature that are normally around 150–300 °C for weak-mild acid sites and 300–400 °C for strong acid sites [38,39]. According to the integrated area values for the desorption curve the trend of materials total acidity can be described as follows: Cat-In[0.25] > Al_2O_3 > Cat-Ref > Cat-In[0.5] > Cat-In[0.75] > Cat-In[1]. This trend shows how, with the exception of Cat-In[0.25], indium addition reduces the total acidity of the catalyst. Furthermore if the population of the strong acid sites is considered, a trend is observed that is proportional to the In loading: Al_2O_3 > Cat-Ref > Cat-In[0.25] > Cat-In[0.5] > Cat-In[0.75] > Cat-In[1]. This diminution of the population of strong acid sites, as also reported by Jahel et al. [39], is probably due to the formation of In aluminates during the thermal treatment steps of the synthesis, leading to the neutralisation of some acidic sites on the alumina support. This hypothesis is supported by H_2-TPR analysis (Fig. 5A), which shows higher hydrogen uptake in the high temperature zone (600–800 °C) that could be related to the formation of indium-aluminate species. The total acidic sites decreasing with the addition of In is in agreement with the experimental results of Liu et al. [40], Passos et al. [41] and Rodríguez-González et al. [42]. Those results suggests that the loading of indium component can partly neutralise the acid sites, especial the stronger acid sites of support and therefore in terms of reactivity it is expected that the indium-containing catalysts should be more selective towards dehydrogenation reducing undesired cracking reactions.

The profiles of reduction under hydrogen for the catalysts are reported in Fig. 5 and show three different zones of hydrogen uptake: a first well designated region, centred at 250 °C, a second in the range of 350–540 °C and a third at higher temperature (550–800 °C) that is present only for the catalyst with high indium content (Cat-In[0.5], Cat-In[0.75], Cat-In[1]). In accordance with the results reported in the literature, the first peak is attributed to the reduction of Pt oxides and/or an oxy-chloro-platinum surface complex [PtO_xCl_y] and, possibly, to the reduction of Sn oxide. The reduction of surface platinum takes place in the range 150–200 °C, Pt species in a stronger interaction with the support can reduce at higher temperatures (200–300 °C) [39,43], while reduction of Sn(IV) to Sn(II) can also contribute, as is reported to take place at (200–300 °C) in presence of Pt catalysing the reduction [27]. The presence of indium is indicated by the increase of the first peak area, particularly accentuated when passing from the concentration (w/w) of 0.25% to 0.5%. This change in the profile can be attributed to reduction of a fraction of In oxide shifted at lower temperature due to a close Pt-In interaction (possibly forming Pt_xIn alloys), or an effect of indium reinforcing the Pt-Sn interaction and leading to a higher amount of Pt_xSn alloys. This hypothesis is in

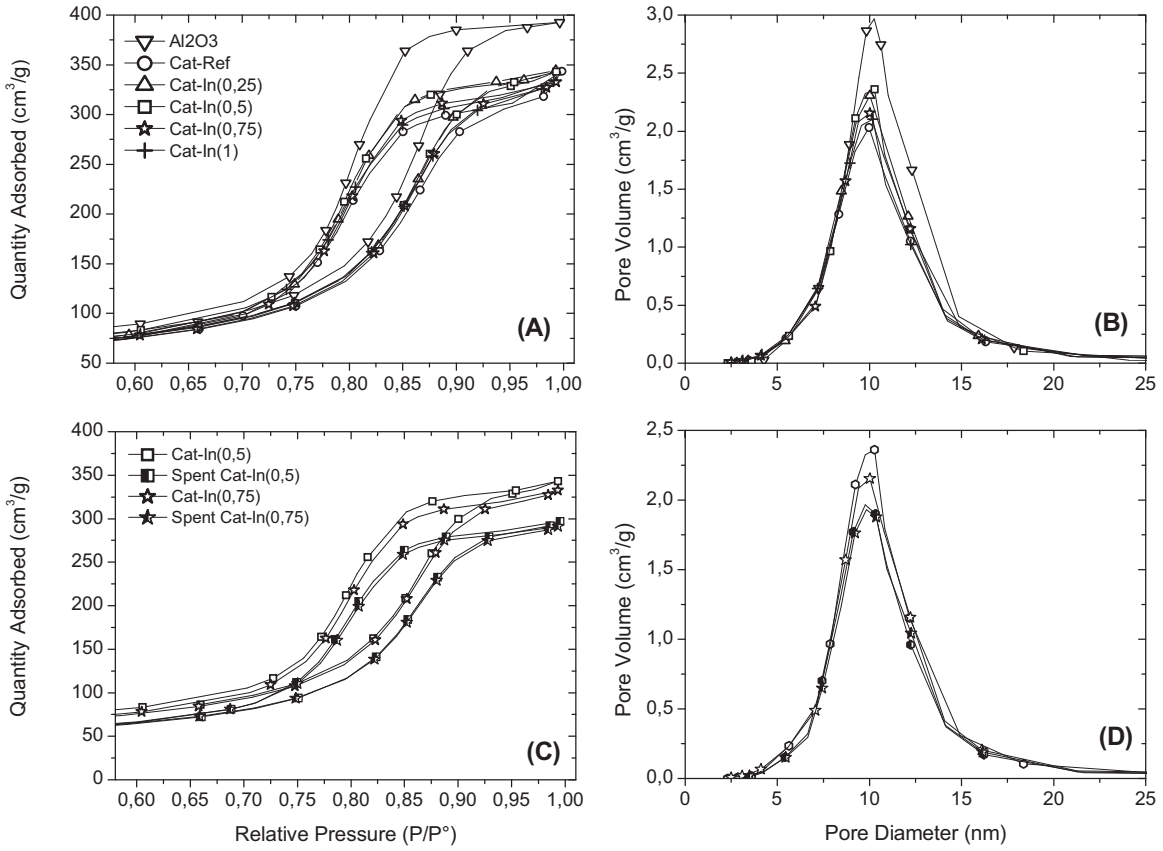

Fig. 3. Nitrogen adsorption/desorption isotherms (A and C) and pore diameter distribution (B and D) for the fresh and spent materials.

agreement with the results obtained by Jahel et al. [39] using Mössbauer spectroscopy, showing that with the increase of the indium content the signal related to Pt_xSn alloys also augments. The second zone of hydrogen uptake at 380–400 °C with a shoulder at 450 °C is interpreted as the reduction of Sn and In oxides competing with each other: reduction of In oxide on Al_2O_3 should take place around 430 °C while Sn oxide in strong interaction with the support at about 550 °C; the fact that both are shifted towards lower temperatures could be due to competition for reactive alumina sites, resulting in a weaker interaction with the alumina therefore an easier reduction [39]. The third zone of hydrogen uptake (550–800 °C) that is present only for the catalysts with In content higher than 0.25% is ascribed to the reduction of indium-aluminate species.

The values of metal dispersion and average metal particle size are calculated from the H_2 chemisorption analysis and are reported in Table 1. The dispersion obtained is similar for all the samples (45–50%) except for Cat-In[1] that displays a lower value (36%). Those values are an index of the accessibility of Pt atoms and indicate that a high indium loading decrease the amount of H_2 chemisorpted by geometric effects or alloy formation. The dispersion values are in good agreement with the catalyst activity with

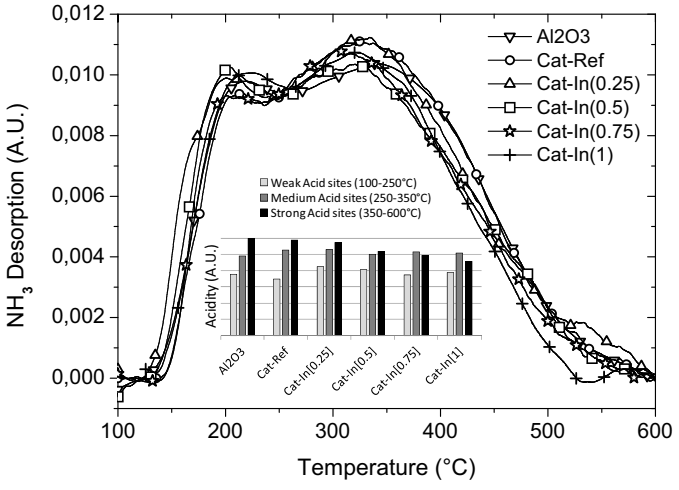

Fig. 4. NH_3-TPD profiles of the fresh materials and distribution of acid sites strength by integration.

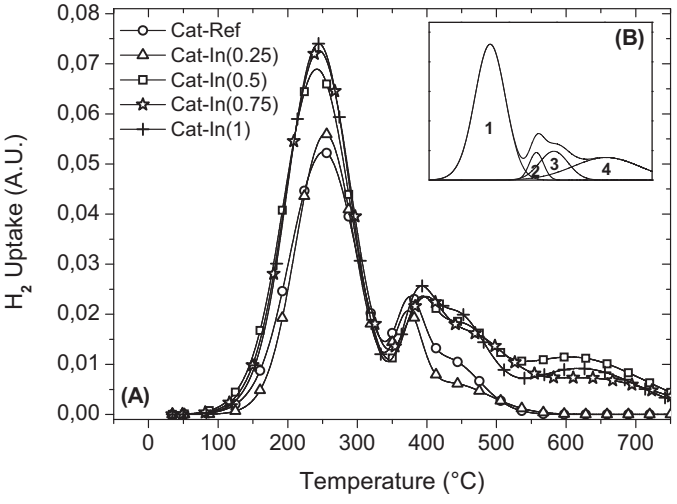

Fig. 5. H_2-TPR profiles of the fresh materials (A) and an example of peak deconvolution (B).

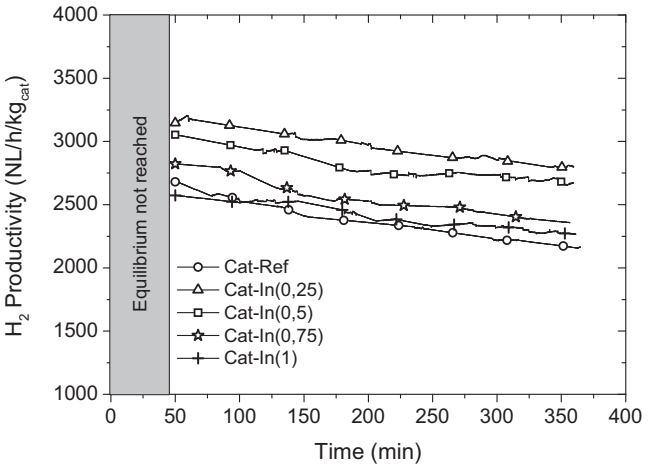

Fig. 6. Hydrogen productivity evolution during reaction.

the highest value corresponding to the most performing catalyst Cat-In[0.5]. The calculated average particle size is in the range 2.3–3.2 nm. It has to be considered though, that the main factor responsible for hydrogen adsorption at room temperature in chemisorption measurements is the fraction of unalloyed Pt, rather than the Pt in alloy with Sn. As a consequence, it is difficult to tell whether the small differences between dispersion values are caused by a different amount of Pt-Sn alloy or by the actual particle size [43].

3.2. Catalytic testing results

Catalyst testing results reported in Fig. 6 show the evolution of hydrogen productivity relative to reaction time. The hydrogen production during the first 45 min is not shown as the equilibrium in the catalytic system is not reached; therefore, the values are not representative of the actual activity at time zero. Hydrogen productivity is expressed in litres at normal conditions for each hour of reaction per kg of catalyst (NL h^{-1} kg^{-1}).

The reactivity of the catalysts is a combined effect of the activity of metal sites (that catalyse the dehydrogenation reactions) and the acid sites (isomerisation, cyclisation reactions on weak-mild acid sites and cracking reactions on strong acid sites) [44]. Overall the materials activity may be described as follows: the catalyst that presents highest hydrogen yield is Cat-In[0.25], nevertheless the best compromise between hydrogen productivity, and purity, and catalyst stability is given by Cat-In[0.5]. The catalysts having highest indium content (0.75% and 1%) show enhanced stability with respect to the reference catalyst Cat-Ref, but the hydrogen productivity decreases. As suggested also by Benitez et al. [45] in a previous study on trimetallic catalysts, this effect could be caused by an excessive loading of indium that partially occludes platinum particles, limiting reactant accessibility to the active dehydrogenation sites.

Comparing data derived from NH_3-TPD (Fig. 4) and catalyst testing results (Fig. 6) it is noted that lower H_2 productivity is associated with the diminution of weak-mild acid sites; those, together with Pt sites, can catalyse dehydrocyclisation of linear paraffins [46], leading to the formation of cyclic hydrocarbons and subsequently to H_2 and aromatics [23], explaining the correlation between indium content and productivity. It has been observed that, with exception of Cat-In[0.25] where there is an increased number of weak-mild acid sites, addition of higher amounts of indium leads to diminution of acidity; this effect together with the hindering effect of Pt particles by Sn and In could explain the trend in H_2 productivity for these materials.

Similarly, comparing H_2-TPR profiles (Fig. 5) and the productivity (Fig. 6), it is also observed that increased In loading leads to a stronger interaction between Pt and Sn (probably with formation of more Pt alloys) (Section 3.1), which could explain why indium addition enhances catalysts stability: there is much evidence in the literature showing that interaction between Pt and Sn leads to a more stable catalyst because of geometric and/or electronic effects [27,47,48]. Particles of Sn can help the separation between Pt clusters increasing the selectivity towards the dehydrogenation reaction and reducing particle sintering. The electron mobility between Pt and Sn could also modify the bond energy between Pt and adsorbed hydrogen. The relative lifetime of the catalysts is consistent with this hypothesis.

The hydrogen produced by PDh on kerosene has a very high purity that varies between 97.2% and 98.2%. CH_4 is the main by-products, as well as traces of C_3 light hydrocarbons (Table 3). Contrary to what was expected, a slight increase of methane was noticed for the catalysts with a lower content of strong acid sites, in which case the hydrogenolysis reactions should decrease; however, the error on the quantity of C_3 could be considerable because the amounts were very close to the detection limit of the instrument (≈0.1%). The H_2 flow produced is CO free, with the implication that it should be possible to be fed directly to a PEM (proton exchange membrane) fuel cell system without further purification steps, leading to a good efficiency in the conversion to electric energy. A summary of the performance of the catalyst can be found in Table 3.

3.3. Carbon coke characterisation and study

Carbon coke deposition is the main reason for catalyst deactivation during the reaction of partial dehydrogenation of low sulfur jetA-1. Different techniques were used to investigate how indium addition influences the mechanisms of carbon formation leading to active phase deactivation. TGA/DTA, elemental analysis and Raman spectroscopy analysis results were compared with the purpose of having a more precise model of the deactivation phenomena.

All the analyses were performed on spent materials after a 6 h reaction time in order to evaluate the quantity and the nature of the carbon coke formed. The procedure for unloading the catalyst from the reactor was the following: kerosene vapour flow was stopped while an equal volumetric flow of Ar was turned on; after purging the system of kerosene residues, the simulated recycle of H_2 and the heating of evaporator, pre-heater and reactor were turned off.

Table 3
Materials performance and catalytic properties.

Material	Lifetime (h)[a]	Deactivation (%)[b]	H_2 purity (%)	H_2 yield (%)	H_2/kerosene (NL/L)	TOF (s^{-1})
Cat-Ref	34.8	16.5	98.2	5.7	79.5	0.58
Cat-In[0.25]	48.9	13.9	98.1	6.5	88.1	0.73
Cat-In[0.5]	107.1	11.8	97.8	6.4	86.7	0.69
Cat-In[0.75]	43.6	17.4	97.4	5.5	76.3	0.63
Cat-In[1]	52.4	14.0	97.2	5.5	76.7	0.59

[a] Linear extrapolation (180–360 min TOS).
[b] Ratio initial/final H_2 productivity.

Table 4
Carbon coke characterisation.

Material	TGA/DSC coke (%)	Coke 1st peak area (a.u.)[a]	Coke 2nd peak area (a.u.)[a]	E.A. total (%)	E.A. carbon (%)	E.A. hydrogen (%)	E.A. C/H	Ordered/ disordered coke[b]
Cat-Ref	3.2	12.3	6.9	3.0	2.4	0.6	4.0	0.68
Cat-In[0.25]	3.0	11.8	10.2	2.9	2.3	0.6	3.8	0.61
Cat-In[0.5]	2.6	10.5	7.6	2.7	2.1	0.6	3.5	0.56
Cat-In[0.75]	2.1	10.8	7.4	2.0	1.4	0.6	2.3	0.44
Cat-In[1]	2.1	11.4	5.5	2.0	1.4	0.6	2.3	0.47

[a] Deconvolution of DTA signal.
[b] Deconvolution of Raman signal.

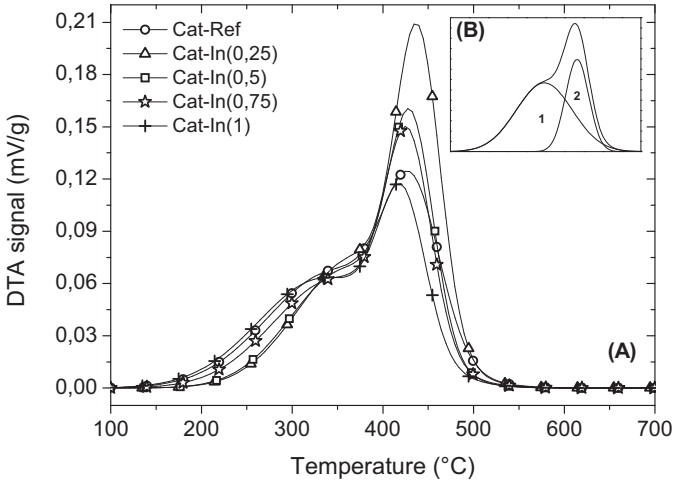

Fig. 7. DTA signal evolution recorded during TG analysis of the spent catalysts (A) and an example of peak deconvolution (B).

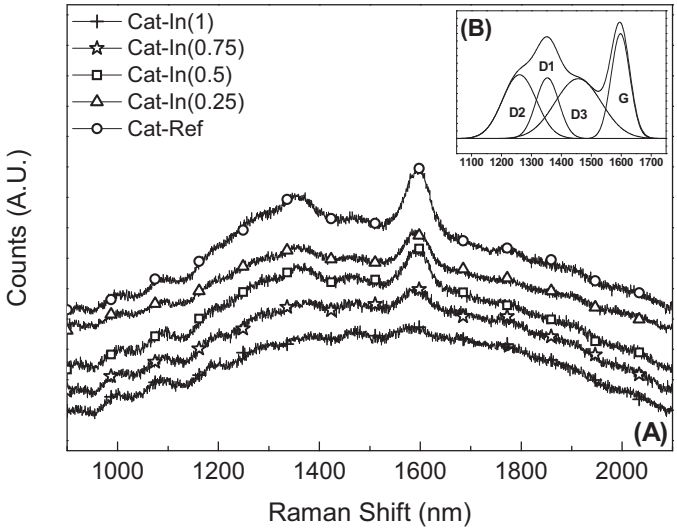

Fig. 8. Raman spectra of the spent catalysts (A) and an example of peak deconvolution (B).

When the system had cooled down the catalyst was discharged and degassed to eliminate absorbed kerosene.

Table 4 lists the amount of carbon coke formed during the reaction obtained for the spent catalysts. Indium addition has a beneficial effect, reducing the amount of carbon deposited during the reaction even when it is present in small amounts. From the differential thermal analysis plot (Fig. 7) it may be observed that the exothermic peaks of coke combustion seem to be the result of two different contributions, with a peak at lower temperature (300–350 °C) and one at higher temperature (400–450 °C). After deconvolution and integration of the two contributions, a linear correlation emerged between the area of the first peak and catalyst lifetime, while the second peak seems to be related to the acidity of the material. In line with previous studies on carbon coke deposits [49,50], we assume that the first peak is related to coke formed on the active metal phase and the second peak to coke formed on acid sites of the alumina support. The first type of carbon burns at lower temperature because its oxidation is promoted by the proximity of Pt particles and it is the major factor for catalyst deactivation as this carbon "covers" the active phase. The second type of coke is in strong interaction with the support and burns at a higher temperature; it affects the deactivation much less because it does not interact directly with the active phase. However, it could hinder access to active sites by pore and channel clogging, but, as seen from catalytic tests and porosity analysis on spent materials, the amount of carbon seems to be insufficient to produce such an effect. The effect of indium is then to diminish the quantity of carbon coke formed on the active phase, thus increasing the lifetime of the catalysts. It has also been hypothesised that the presence of indium can facilitate the migration of the carbon from the active phase towards the support, helping this way to keep the active sites reactive. There is evidence in the literature of coke migration from the active metal to the support for bimetallic Pt catalyst [51]. In particular Vu et al. [52] observed that carbon coke mobility on the catalyst surface of Pt-Sn/Al_2O_3 is related to the presence of different Pt_xSn alloys. As noticed from H_2-TPR analysis (Section 3.1) the presence of indium seems to increase the amount of Pt_xSn alloys formed, which suggests that the effect of coke migration from the active phase to the support could contribute to the better stability of indium doped catalysts.

CNHS elemental analysis results, listed in Table 4, are in good correlation with the values obtained by TG analysis giving a confirmation on the reliability of the carbon coke study. No trace of sulfur was found in the deposit and the graphitisation of the coke calculated as ratio between C/H (w/w) is proportional to the total amount of coke formed.

In order to complete the study of the carbon coke formed during PDh reaction, Raman spectroscopy has been performed on the spent catalysts. This technique presents some difficulties related to interference by fluorescence caused by some aromatics and polyaromatics present in the carbon, but with a fine tuning of the instrument parameters the spectra reported in Fig. 8 were obtained. For the catalysts containing a high amount of coke (Cat-Ref, Cat-In[0.25]) the peaks related to ordered carbon D1 (1350 nm) and G (1590 nm) are clearly visible, while other peaks decreased. The ratio between ordered and disordered carbon has been calculated as the ratio between the area of D1 + G peaks and the other peaks [53] obtaining a good correlation with the graphitisation ratio previously calculated from elemental analysis data (Table 4).

4. Conclusions

The effect of addition of indium to the well known system based on Pt-Sn/Al_2O_3 has been investigated. The reducibility of the active phase is improved and the activity towards the dehydrogenation reaction is increased. The number of strong acid sites is reduced, so avoiding undesired side reactions such as cracking, and consequently decreasing carbon coke formation and improving catalyst stability. The presence of indium also diminishes the amount of coke formed in the proximity of Pt particles, which serves to stabilise the catalyst activity. The catalyst Cat-In[0.5] with metal ratio of 0.5:1:1 In:Pt:Sn has been identified as the best compromise between catalyst activity and stability. This catalyst allows the production of a hydrogen flow (purity 97.8%) of 2900 NL h^{-1} $kg_{cat}{}^{-1}$ corresponding to 86.7 NL $L_{kerosene}{}^{-1}$ that can generate around 2.9 kW electricity (assuming a 50% efficiency for PEM fuel cell). The hydrogen yield is about 6.5% and is generated mainly from dehydrogenation of cycloalkanes to aromatics. This degree of conversion should allow the utilisation of partially dehydrogenated kerosene as combustible fuel.

Acknowledgement

The authors acknowledge the financial support of the European Union under the GreenAir project (Grant Agreement 233862) within the European Community's Seventh Framework Programme. The authors thank Sasol Germany for providing the alumina support.

References

[1] Key World Energy Statistics 2012, International Energy Agency, https://www.iea.org/publications/freepublications/publication/kwes.pdf
[2] H. Larsen, L. Sønderberg Petersen, Risø Energy Report 9, 2010, http://www.cphcleantech.com/media/2100721/ris%C3%B8%20energy%20report%209.pdf
[3] US Department Of Energy (DOE), Hydrogen and fuel cells program plan, 2010, http://www.hydrogen.energy.gov/pdfs/program_plan2011.pdf
[4] U. Eberle, M. Felderhoff, F. Schüth, Angew. Chem. Int. Ed. 48 (2009) 6608.
[5] D. Mori, K. Hirose, Int. J. Hydrogen Energy 34 (2009) 4569–4574.
[6] S. Yolcular, Ö Olgun, Catal. Today 138 (2008) 198–202.
[7] R.B. Biniwale, S. Rayalu, S. Devotta, M. Ichikawa, Int. J. Hydrogen Energy 33 (2008) 360–365.
[8] A. Shukla, J.V. Pande, R.B. Biniwale, Int. J. Hydrogen Energy 37 (2012) 3350–3357.
[9] Airbus S.A.S. Customer Service, A320 Aircraft Characteristics Airport And Maintenance Planning 2005, http://www.airbus.com/fileadmin/media_gallery/files/tech_data/AC/Airbus-AC-A320-Jun2012.pdf
[10] Breit, J. Office of Energy Efficiency and Renewable Energy (EERE), DOD-DOE Fuel-Cell APUWorkshop 2010, http://www1.eere.energy.gov/hydrogenandfuelcells/pdfs/aircraft_6_breit.pdf
[11] Y. Okada, E. Sasaki, E. Watanabe, S. Hyodo, H. Nishijima, Int. J. Hydrogen Energy 31 (2006) 1348–1413.
[12] N. Kariya, A. Fukuoka, T. Utagawa, M. Sakuramoto, Y. Goto, M. Ichikawa, Appl. Catal. A 247 (2003) 247–259.
[13] S. Hodoshima, N. Hiroaki, S. Yasukazu, Appl. Catal. A 292 (2005) 90–96.
[14] R.B. Biniwale, N. Kariya, M. Ichikawa, Catal. Lett. 105 (2005) 83–87.
[15] Y. Wang, N. Shah, F.E. Huggins, G.P. Huffman, Energy Fuels 20 (2006) 2612–2615.
[16] D. Sebastian, E.G. Bordejé, L. Calvillo, M.J. Lazaro, R. Moliner, Int. J. Hydrogen Energy 33 (2008) 1329–1334.
[17] K. Akamatsu, Y. Ohta, T. Sugawara, T. Hattori, S. Nakao, Ind. Eng. Chem. Res. 47 (2008) 9842–9847.
[18] P.D. Tien, T. Satoh, M. Miura, M. Nomura, Fuel Process. Technol. 89 (2008) 415–418.
[19] P. Li, Y. Huang, D. Chen, J. Zhu, T. Zhao, X. Zhou, Catal. Commun. 10 (2009) 815–818.
[20] M.P. Lazaro, E. Garcia-Bordejé, D. Sebastian, M.J. Lazaro, R. Moliner, Catal. Today 138 (2008) 203–209.
[21] Á. Reyes Carmona, E. Gianotti, M. Taillades-Jacquin, G. Taillades, J. Rozière, E. Rodríguez-Castellón, D.J. Jones, Catal. Today 210 (2013) 26–32.
[22] M. Taillades-Jacquin, C. Resini, K.E. Liew, G. Taillades, I. Gabellini, D. Wails, J. Rozière, D.J. Jones, Appl. Catal., B 142–143 (2013) 112–118.
[23] C. Lucarelli, S. Albonetti, A. Vaccari, C. Resini, G. Taillades, J. Rozière, K. ELiew, A. Ohnesorge, C. Wolff, I. Gabellini, D. Wails, Catal. Today 175 (2011) 504–508.
[24] C. Resini, C. Lucarelli, M. Taillades-Jacquin, K.E. Liew, I. Gabellini, S. Albonetti, D. Wails, J. Rozière, A. Vaccari, D.J. Jones, Int. J. Hydrogen Energy 36 (2011) 5972–5982.
[25] B. Wang, G.F. Froment, D.W. Goodman, J. Catal. 253 (2008) 239–243.
[26] C.H. Bartholomew, Appl. Catal. A Gen. 212 (2001) 17–60.
[27] S. He, C. Sun, Z. Bai, X. Dai, B. Wang, Appl. Catal. A Gen. 356 (2009) 88–98.
[28] M.P. González-Marcos, B. Iñarra, J.M. Guil, M.A. Gutiérrez-Ortiz, Catal. Today 107–108 (2005) 685–692.
[29] V.A. Mazzieri, J.M. Grau, J.C. Yori, C.R. Vera, C.L. Pieck, Appl. Catal. A Gen. 354 (2009) 161–168.
[30] S. Sahebdelfar, M.T. Ravanchi, F.T. Zangeneh, S. Mehrazma, S. Rajabi, Chem. Eng. Res. Des. 90 (2012) 1090–1097.
[31] F.T. Zangeneh, S. Mehrazma, S. Sahebdelfar, Fuel Process. Technol. 109 (2012) 118–123.
[32] V.A. Mazzieri, J.M. Grau, C.R. Vera, J.C. Yori, J.M. Parera, C.L. Pieck, Appl. Catal. A Gen. 296 (2005) 216–221.
[33] L.S. Carvalho, C.L. Pieck, M.C. Rangel, N.S. Fígoli, J.M. Grau, P. Reyes, J.M. Parera, Appl. Catal. A Gen. 269 (2004) 91–103.
[34] L.S. Carvalho, C.L. Pieck, M.C. Rangel, N.S. Fígoli, C.R. Vera, J.M. Parera, Appl. Catal. A Gen. 269 (2004) 105–116.
[35] S.A. Bocanegra, A.A. Castro, O.A. Scelza, S.R. de Miguel, Appl. Catal. A Gen. 333 (2007) 49–56.
[36] F.T. Zangeneh, S. Mehrazma, S. Sahebdelfar, Fuel Process. Technol. 109 (2013) 118–123.
[37] B.K. Vua, M.B. Songa, I.Y. Ahnb, Y.W. Suhb, D.J. Suhb, W.I. Kimc, H.L. Kohc, Y.G. Choic, E.W. Shina, Appl. Catal. A Gen. 400 (2011) 25–33.
[38] Y. Zhang, Y. Zhou, X. Sheng, L. Wan, Y. Li, Y. Xiao, B. Yu, Z. Zeng, Fuel Process. Technol. 104 (2012) 23–30.
[39] A. Jahel, P. Avenier, S. Lacombe, J. Olivier-Fourcade, J.C. Jumas, J. Catal. 272 (2010) 275–286.
[40] A. Gervasini, J.A. Perdigon-Melon, C. Guimon, A. Auroux, J. Phys. Chem. B 110 (2006) 240–249.
[41] F.B. Passos, D.A.G. Aranda, M. Schmal, J. Catal. 178 (1998) 478–488.
[42] V. Rodríguez-González, R. Gómez, M. Moscosa-Santillan, J. Amouroux, J. Sol–Gel. Sci. Technol. 90 (2007) 331–338.
[43] S.M. Stagg, C.A. Querini, W.E. Alvarez, D.E. Resasco, J. Catal. 168 (1997) 75–94.
[44] V.A. Mazzieri, J.M. Grau, C.R. Vera, J.C. Yori, J.M. Parera, C.L. Pieck, Catal. Today 107–108 (2005) 643–650.
[45] V.M. Benitez, C.R. Vera, M.C. Rangel, J.C. Yori, J.M. Grau, C.L. Pieck, Ind. Eng. Chem. Res. 48 (2009) 671.
[46] A.A. Ali, L.I. Ali, S.M. Aboul-Fotouh, A.K. Aboul-Gheit, Appl. Catal. A Gen. 215 (2001) 161–173.
[47] S. He, W. Bi, Y. Lai, X. Rong, X. Yang, C. Sun, J. Fuel Chem. Technol. 38 (4) (2010) 452–457.
[48] M.L. Yang, Y.A. Zhu, X.G. Zhou, Z.J. Sui, D. Chen, ACS Catal. 2 (2012) 1247–1258.
[49] F.T. Zangeneh, S. Sahebdelfar, Iran J. Chem. Chem. Eng. 8 (2011) 3.
[50] K.M. Hardiman, C.G. Cooper, A.A. Adesina, R. Lange, Chem. Eng. Sci. 61 (2006) 2565.
[51] S.I. Sanchez, M.D. Moser, S.A. Bradley, ACS Catal. 4 (2014) 220–228.
[52] B.K. Vu, M.B. Song, I.Y. Ahn, Y. Suh, D.J. Suh, W. Kim, H. Koh, Y.G. Choi, E.W. Shin, Appl. Catal. A Gen. 400 (2011) 25–33.
[53] S. He, C. Sun, X. Yanga, B. Wang, X. Dai, Z. Bai, Chem. Eng. J. 163 (2010) 389.